Title

Sputtered p-Type Cu x Zn1–x S Back Contact to CdTe Solar Cells

Journal

ACS Applied Energy Materials, 3(6)

ISSN

2574-0962

Authors

Woods-Robinson, Rachel
Ablekim, Tursun
Norman, Andrew
et al.

Publication Date

2020-06-22

DOI

10.1021/acsaem.0c00413

Peer reviewed

Sputtered p-type $Cu_xZn_{1-x}S$ Back Contact to CdTe Solar Cells

Rachel Woods-Robinson,[*,†,‡,¶] Tursun Ablekim,[¶] Andrew Norman,[¶] Steve Johnston,[¶] Kristin A. Persson,[†,‡] Matthew O. Reese,[¶] Wyatt K. Metzger,[¶] and Andriy Zakutayev[*,¶]

†*University of California Berkeley, Berkeley, CA 94702, USA*

‡*Lawrence Berkeley National Laboratory, Berkeley, CA 94720, USA*

¶*National Renewable Energy Laboratory, Golden, CO 80401, USA*

E-mail: rwoodsrobinson@lbl.gov; Andriy.Zakutayev@nrel.gov

Keywords: CdTe photovoltaics, copper zinc sulfide, solar cell back contact design, transparent semiconductors, solar cell interfaces

Abstract

As thin film cadmium telluride (CdTe) solar cells gain prominence, one particular challenge is optimizing contacts and their interfaces to transfer charge without losses in efficiency. Back contact recombination is still significant and will prevent CdTe solar technology from reaching its full potential in device efficiency, and transparent back contacts have not been developed for bifacial solar technology or multijunction solar cells. To address these challenges, this study investigates sputtered $Cu_xZn_{1-x}S$ as a p-type semi-transparent back contact material to thin film polycrystalline CdTe solar cells, at Cu concentrations x = 0.30, 0.45 and 0.60. This material is selected for its high hole conductivity (160 to 2,120 S cm^{-1}), wide optical band gap (2.25 to 2.75 eV), and variable

ionization potential (approximately 6 to 7 eV) that can be aligned to that of CdTe. We report that without device optimization, CdTe solar cells with these $Cu_xZn_{1-x}S$ back contacts perform as well as control cells with standard ZnTe:Cu back contacts. We observe no reduction in external quantum efficiency, low contact barrier heights of approximately 0.3 eV, and carrier lifetimes on par with those of baseline CdTe. These cells are relatively stable over one year in air, with V_{OC} and efficiency of the $x = 0.30$ cell decreasing by only 1% and 3%, respectively. Using SEM and STEM to investigate the $Cu_xZn_{1-x}S-CdTe$ interface, we demonstrate that the $Cu_xZn_{1-x}S$ layer segregates into a bilayer of Cu-Te-S and Zn-Cd-S, and thermodynamic reaction calculations support these findings. Despite its bilayer formation, the back contact still functions well. This investigation explains some of the physical mechanisms governing the device stack, inspires future work to understand interfacial chemistry and charge transfer, and elicits optimization to achieve higher efficiency CdTe cells.

Introduction

Cadmium telluride (CdTe) solar cell devices have reached efficiencies up to 22.1%,[1] and are the most dominant thin film photovoltaic (PV) technology on the market today.[2] However, several materials challenges remain that prevent this technology from meeting its theoretical detailed balance limit efficiency of 30%.[3] One such challenge is the identification and implementation of buffer layers (also called contact layers, carrier selective contacts, carrier transport layers, etc.) that are adequately aligned to the absorber such that photogenerated charge carriers are efficiently collected and transported out of the device with minimal losses.[4,5] Prominent contact materials in commercial and research-grade superstrate CdTe cells are Cd(O,S)[6,7] or $Mg_xZn_{1-x}O$[8,9] for the electron selective front interface and Cu:ZnTe for the hole selective back interface.[10–12] However, interfacial losses due to Schottky barrier formation and recombination will prevent CdTe solar technology from reaching its full potential.[5,13] Back contact barrier heights have been reported of ∼0.3–0.5 eV for Cu:ZnTe

back contact cells, and Cu migration can lead to changes in series resistance and fill factor, causing stability issues.[14–16]

Thus, development of a semi-transparent hole selective contact with adequate interfacial alignment to CdTe could lead to higher future conversion efficiencies. Furthermore, CdTe is currently limited to a superstrate configuration of p-type CdTe with an n-type emitter and transparent n-type top contact; this is in part because of the lack of a p-type transparent conductor aligned to CdTe's high work function of approximately 5.7 eV.[17] Such a material could enable a variety of novel CdTe device configurations including a substrate configuration, top cell configuration in tandem PV, and bifacial PV devices.[18]

Here, we focus on hole selective back contacts to conventional superstrate CdTe devices. According to the literature, future back contacts require the following key design criteria, which serve as guidelines for this study:

1. **Hole concentration:** The hole concentration should place the Fermi energy E_F (i.e. chemical potential at 0 K) of the back contact close to or within the CdTe valence band maximum (VBM) such that it is sufficiently p-type doped. The exact hole density depends on absorber hole density, so tunability of hole concentration could also be advantageous.

2. **VBM alignment:** The VBM of the back contact preferably should be aligned within approximately 0.0-–0.3 eV of CdTe's VBM to prevent barrier effects.[19]

3. $\boldsymbol{E_F}$ **alignment:** The initial Fermi level offset should be *positive* such that the E_F of the back contact material is *below* that of CdTe at zero bias.[19]

4. **Electron reflection:** The conduction band minimum (CBM) of the back contact should be higher in energy than the CdTe CBM such that electrons are reflected at the interface. This suggests a band gap E_G greater than the CdTe band gap of approximately 1.5 eV (c.f. Condition 2).

5. **Interfacial chemical stability:** The interface between CdTe and the back contact should be stable, without spurious reactions and formation of a detrimental secondary phase.

6. **Passivation:** The contact should be passivating such that it does not introduce recombination-inducing defects into the CdTe absorber.[5,13]

Maintaining a low thermal budget (synthesis less than ∼200 °C) is usually preferable to avoid thermal reconstruction at the interface, especially for thin film polymer contacts, but this condition depends on the specific device configuration so is not included above. Cu-free contacts is another possible criterion the community is moving towards.

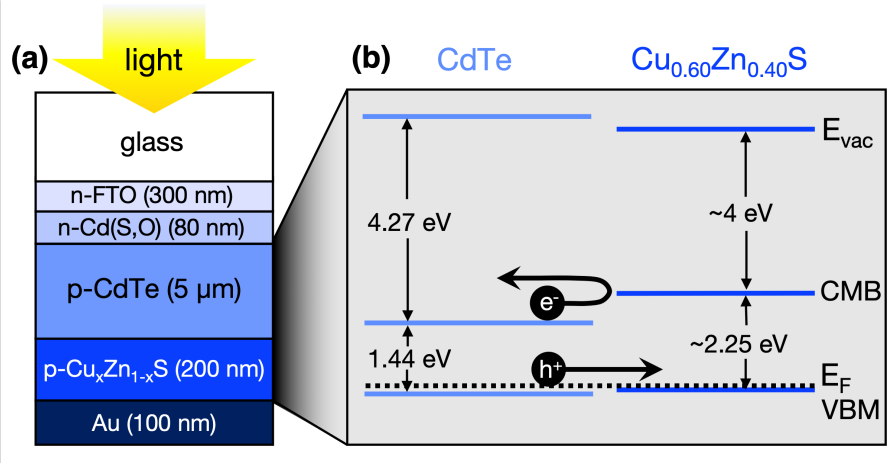

Figure 1: (a) Schematic of the as-deposited superstrate polycrystalline CdTe solar cells investigated in this study, with $Cu_xZn_{1-x}S$ as a p-type back contact (not to scale). (b) Approximate alignment of the as-deposited CdTe−$Cu_xZn_{1-x}S$ interface for x = 0.60 under zero bias, guiding our selection of this material system. Note that the electron affinity of $Cu_xZn_{1-x}S$ is an estimate based on Figure 2, band bending at the interface is not included, and the x-axis (thickness) is not to scale.

In the early days of CdTe, metal contacts were applied directly to the absorber but resulted in Schottky barriers due to CdTe's high work function, so "buffer" back contacts such as Cu:ZnTe are now used. Researchers over the past decades have also investigated alternate back contact materials to Cu:ZnTe, primarily Cu containing contacts e.g. Cu_xTe,[20–22] Cu_xS,[23–25] Cu:HgTe,[26] CuI,[27] CuSCN,[28] and Cu nanowires with graphene,[29] with a

variety of different metallization schemes. Non-Cu-containing contacts have also been explored, e.g. Sb_2Te_3,[30–32] As_2Te_3,[33] FeS_2,[34] MoO_x,[35,36] NiO_x,[37] Ni:P,[38] and ZnTe, but results are not definitive and efficiencies are usually lower than Cu-containing counterparts unless the absorber utilizes group V dopants.[33,39] None of these materials have yet resulted in a completely loss-free Ohmic hole transport and electron reflecting buffer layer, so formation of a chemically stable barrier-free back contact without recombination remains a grand challenge.

One material space that warrants exploration in CdTe is the ternary chalcogenide $Cu_xZn_{1-x}S$ – also written ZnS:Cu_yS to indicate a composite, or Cu-Zn-S to indicate full ternary space – which has been gaining traction as a wide gap p-type semiconductor for photovoltaic and optoelectronic applications.[40–42] Its optoelectronic properties are highly tunable within cation chemical potential space, allowing for band gaps between 2.4 eV and 3.4 eV,[43] and hole conductivities ranging orders of magnitude (reported up to 1,000 S cm^{-1} for $x = 0.65$)[41]. Development of facile chemical bath deposition (CBD) and incorporation into np^+:Si devices as a transparent hole selective contact with V_{OC} up to 535 mV demonstrated its potential PV applications.[41] One of the most remarkable properties of the $Cu_xZn_{1-x}S$ system is the ability for enhanced properties and high crystallinity even at low synthesis temperatures, compatible with the thermal budget of CdTe, as well as its strong chemical and aqueous stability despite being a sulfide. Nanocomposite CBD synthesis of ZnS:Cu_yS has been recently investigated as a back contact to polycrystalline p-type CdTe,[44] but this configuration still relies on ITO for carrier transport. Additionally, this synthesis method has a limited range of thickness tunability. CBD-synthesized ZnS:Cu_yS has also been studied as a top contact to n-type CdTe,[45] but nonuniform film quality leading to pinhole formation was problematic. Neither study investigated device stability or interfacial chemistry.

In this study, we explore sputtered $Cu_xZn_{1-x}S$ as a p-type back contact to polycrystalline CdTe solar cells. We focus on sputtered layers rather than CBD to enhance film quality and finely control thickness. The CdTe solar cell film stack is depicted in **Figure 1**(a) where

$Cu_xZn_{1-x}S$ is the as-deposited back contact. We report a high V_{OC} of 837 mV at x = 0.30, efficiencies commensurate with control samples, strong stability in air over one year for all devices and high carrier lifetimes. We additionally investigate the CdTe$-Cu_xZn_{1-x}S$ interface with cross-sectional microscopy, demonstrate a bilayer phase segregation, use first principles calculations to assess thermochemical stability, and suggest pathways for improved device performance.

Methodology

Device Fabrication

Polycrystalline CdTe thin film solar cell devices with a superstrate configuration were fabricated using commercially available FTO-coated Pilkington TEC-12D glass substrates. An 80 nm n-type Cd(S,O) layer was sputtered from a 3" target in a 6% O_2/Ar environment. CdTe was deposited in a closed-space sublimation (CSS) system with a source-to-substrate distance of 3 mm and source and substrate temperatures of 660 °C and 600 °C, respectively. After CdTe deposition, the samples were annealed in $CdCl_2$ treatment at 420 °C for 10 minutes in a separate CSS chamber,[46] and residual $CdCl_2$ was rinsed off in DI water after the treatment. No other surface treatment was pursued other than water rinsing.

$Cu_xZn_{1-x}S$ was then RF co-sputter deposited at ambient temperature on the CdTe absorber from 50 mm diameter zincblende ZnS and chalcocite Cu_2S targets. $Cu_xZn_{1-x}S$ standards were also deposited on glass for characterization, and we have recently reported similar films on glass substrates.[43] The compositions used in this study, x = 0.30, 0.45, and 0.60, were achieved by fixing the ZnS target gun at 40 W and setting the Cu_2S target gun to 20 W, 30 W, and 40 W, respectively. As a finishing step, 100 nm of Au was evaporated for metallization. To make a baseline cell, 2.5 nm Cu followed by 350 nm of ZnTe were sputtered on a CdTe to form a control back contact device. After back contact formation, all of the samples were annealed in a tube furnace at 180 °C with 100 SCCM He flow for 30 mins.

For statistical analysis, 4 to 10 finished devices were fabricated for each composition and an example photograph is shown in the Supporting Information.

Material and Interfacial Characterization

Stoichiometry of the $Cu_xZn_{1-x}S$ layer was quantified using x-ray fluorescence (XRF) and corroborated by Rutherford Backscattering Spectrometry (RBS).[43] Structural analysis was performed with X-ray diffraction (XRD) on a Bruker D8 Discover with a θ–2θ geometry, Cu Kα radiation, and a proportional 2D detector. Hall measurements were performed using a Van der Pauw configuration with indium contacts on corners of square size samples, a 0.31 T magnet, and four point probe contact. Optical characterization is described elsewhere.[43] The interfaces of cleaved devices were analyzed with cross-sectional scanning electron microscopy (SEM), using an FEI field emission (FE) Nova NanoSEM 630 at 2.0 kV, 64 pA current, and a working distance of 5.9 mm. Cross-section scanning transmission electron microscopy (STEM) specimens were prepared using the focused ion beam (FIB) lift out technique with the final Ga^+ ion milling performed at 3 kV. Ga^+ ion FIB damage was subsequently removed using low energy (< 1 kV) Ar^+ ion milling in a Fischione Nanomill with the sample cooled by liquid nitrogen. Scanning transmission electron microscopy (STEM) imaging and energy dispersive x-ray spectrometry (EDS) analysis were performed in a FEI Tecnai F20 UltraTwin field emitting gun STEM operated at 200 kV and equipped with an EDAX Octane T Optima Si drift detector (SDD) EDS system.

Device Performance Characterization

After completing the back contact, device areas of 0.25 cm^2 were defined by mechanical scribing. The solar cell devices were tested with current density–voltage (JV) measurements using a Newport solar simulator with AM1.5G filter under one sun conditions. The solar simulator light intensity was calibrated with a GaAs reference cell to match the current readings. External quantum efficiency (EQE) was measured with a 10 nm increment in

wavelength on a Newport (Oriel) IQE 200. Devices were measured on four different occasions over the course of one year under identical experimental conditions.

Current-voltage curves as a function of temperature (JVT) were collected using a current-voltage source/meter (Agilent B2912A) connected to a sample mounted in a closed-cycle helium cryostat. Since samples were deposited on thick glass, a separate temperature sensor was mounted on the top of the sample near the measured device to more accurately record the device temperature. Temperature was swept through the desired range using a temperature controller (Lakeshore 331) that stabilizes the sample temperature to within 1 °C. An automated data collection program was set to maintain a stabilized temperature for one minute before the current-voltage data was collected. Time-resolved photoluminescence (TRPL) measurements were collected using a mode-locked femtosecond pulsed laser with a pulse repetition rate of 1.1 x 10^6 pulses per second. Measurements were performed at open circuit on the glass side of the full device stack (with Au back contacts included). Using an optical parametric amplifier, the laser wavelength was tuned to 640 nm, laser power was 0.1 mW, a dichroic filter was chosen to block reflections and pass long wavelengths, and carrier injection level was approximately 5 $\times$ 10^{16} cm^{-3} (see Supporting Information). A 20X microscope objective was used to focus light and collect PL from a spot diameter of approximately 60 μm. A PicoQuant PicoHarp 300 time-correlated single-photon counting system was used to build up the TRPL decay curve.

Thermodynamic Calculations

The Materials Project's Interfacial Reaction Calculator[47] was used to compute thermodynamic equilibrium reactions and energies based on the computed energies of materials from the Materials Project database.[48] Materials Project Density Functional Theory (DFT) calculations were performed using the projector augmented wave (PAW) method[49,50] as implemented in the Vienna *Ab Initio* Simulation Package (VASP)[51,52] within the Perdew-Burke-Enzerhof (PBE) Generalized Gradient Approximation (GGA) formulation of the exchange-

correlation functional.[53] Cutoff, convergence, and correction criteria are described elsewhere.[48,54] The calculations assume a closed system, where low-temperature (e.g. negligible entropic contributions) and ambient pressure conditions are appropriate.

Results and Discussion

Materials Properties for Device Design

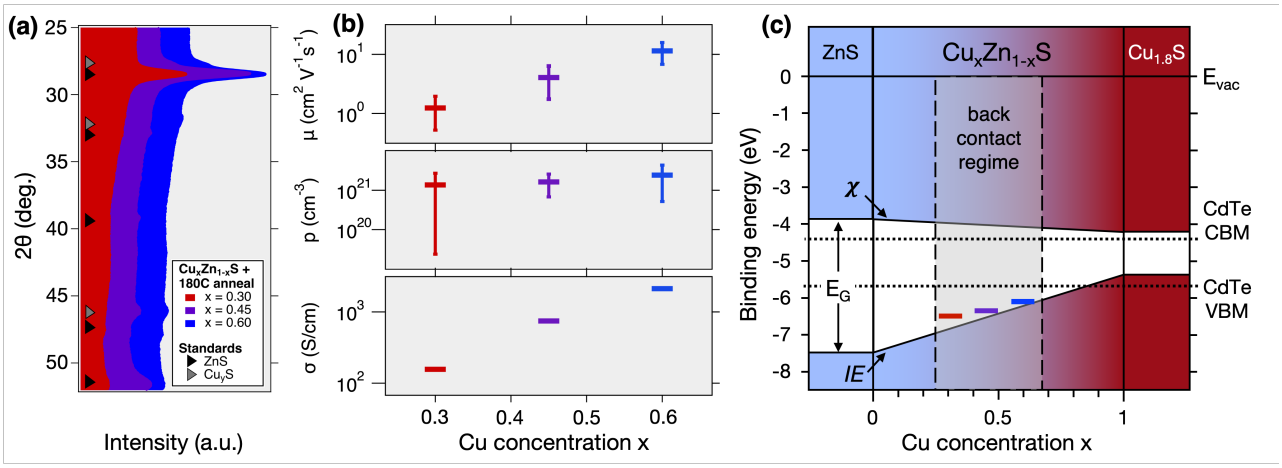

Figure 2: (a) Representative X-ray diffraction (XRD) peaks for $Cu_xZn_{1-x}S$ synthesized at ambient temperature and annealed at 180 °C. (b) Electronic properties for films with x = 0.30, 0.45, and 0.60, where μ is hole mobility, p hole concentration, and σ hole conductivity. (c) Schematic of estimated non-equilibrium band edges within the solid solution phase space of $Cu_xZn_{1-x}S$, with bars corresponding to approximate Fermi levels at the compositions used in devices and dotted lines corresponding to the band edges of CdTe.

In as-deposited sputtered $Cu_xZn_{1-x}S$ films grown at ambient temperature, an alloy has been observed previously across most of the cation chemical composition space, however phase segregation occurred around x = 0.60.[43] Here, sputtered $Cu_xZn_{1-x}S$ films are annealed at 180 °C in He to mimic processing conditions used for CdTe devices, and **Figure 2**(a) illustrates X-ray diffraction (XRD) results. These films phase segregate into zinc blende ZnS and metastable cubic Cu_yS ($Fm\bar{3}m$) ($1 < y < 2$) for x = 0.45 and 0.60, and appear to be single-phase zinc blende alloys for x = 0.30 (the data do not rule out the possibility of phase segregation with nanoscale domains). These films demonstrate strong peaks from zinc

blende ZnS, highly textured in the (111) direction. There may also be traces of wurtzite ZnS, as was observed around x = 0.30 for ambient temperature films,[43] though this phase may destabilize at higher temperatures and due to peak overlaps it is difficult to resolve. Although we demonstrate some phase segregation, this may be acceptable for $Cu_xZn_{1-x}S$ contacts, as has been shown with phase-segregated CBD films.[41,44] Additionally, having one composition where phase segregation is not observed can allow us to compare whether this is in fact detrimental. Herein, we refer to all three compositions as "$Cu_xZn_{1-x}S$" for consistency.

In Figure 2(b) we plot the electronic properties for annealed $Cu_xZn_{1-x}S$ films. The bottom panel indicates that the hole conductivity, σ, increases with Cu concentration from 160 to 2,120 S cm^{-1}. The hole concentration, p, remains relatively constant at $\sim 10^{21}$ cm^{-3}, increasing somewhat with Cu concentration, while hole mobility, μ, increases more prominently with Cu concentration from 1.2 to 11 cm^2 $V^{-1}s^{-1}$.

One major advantage of highly tunable alloys or composites is the ability to tailor optical absorption and band alignment towards desired photovoltaic applications. In Figure 2(c), we assume a linear composition grading between binary endpoints compatible with Vegard's law[55,56] to estimate the range of band gap E_G, electron affinity χ, and ionization potential IE for $Cu_xZn_{1-x}S$. As x increases, we predict relatively constant χ at 3.8–4.0 eV, IE tunable between approximately 7 eV to 6 eV, and E_G tunable from approximately 2.75 eV to 2.25 eV, which corroborates optical measurements reported elsewhere.[41,43] For comparison we show the band offset of CdTe[57] as dotted lines, demonstrating IE values in $Cu_xZn_{1-x}S$ close to or below that of CdTe. In a composite material, the electronic band edges are not well defined, but we retain this schematic as an estimate to guide device integration. This schematic also neglects any alloy band bowing, which would likely lead to VBM positions slightly farther from vacuum (i.e. larger IE). We acknowledge that future x-ray photoelectron spectroscopy experiments are necessary to accurately assess valence band and conduction band positions.

Photovoltaic Device Performance

Figure 2(c) suggests an optimal valence band alignment to CdTe somewhere in the mid-range regime of $0.25 < x < 0.75$, which is denoted the "back contact regime." Accordingly, we use predicted alignments as a guide for selecting the optimal Cu concentration, and then vary the thickness in experiments to achieve desirable transparency or conductivity. Based on the IE estimates, we focus on x = 0.30, 0.45, and 0.60, and layer thicknesses of 200–300 nm. Figure 1(b) illustrates the approximate band offsets at the CdTe$-Cu_xZn_{1-x}S$ interface under no bias for the as-deposited device with x = 0.60. Such an interface follows the back contact design criteria outlined previously; holes should be injected from the CdTe layer into the $Cu_xZn_{1-x}S$, and electrons reflected.

Figure 3(a) plots the JV curves for the three highest performing cells (colored lines) and a baseline cell with a Cu:ZnTe back contact for reference (black dotted line). Derived solar cell performance parameters, namely open-circuit voltage (V_{OC}), short-circuit current (J_{SC}), fill factor (FF), and efficiency (η), are plotted across all cells measured in Figure 3(c-f), respectively. The parameters of the highest performing cells are listed in **Table 1**. The V_{OC} of the $Cu_xZn_{1-x}S$ devices range from ∼834–837 mV. This is nearly as high as the heavily optimized Cu:ZnTe back contact baseline (∼848 mV), and higher than the V_{OC} of $Cu_xZn_{1-x}S$ devices previously reported in the literature.[44] The results indicate that the $Cu_xZn_{1-x}S$ back contact does not appear to affect the front interface adversely through diffusion or other effects. The FF for the x = 0.60 film is even higher than the baseline cells. We note that some J_{SC} values were measured to be greater than 25 mA cm^{-2}, and are likely miscalibrated due to inaccurate measurements of cell area. For this reason, we use EQE to estimate J_{SC} and efficiency, and report these derived values for comparison in Table 1 as "$J_{SC}^{\text{from EQE}}$" and "$\eta^{\text{from EQE}}$" as described in the Supporting Information. The current densities in Figure 3(a) have been calibrated accordingly, but (d) and (f) remain uncalibrated. From this calibration, we observe efficiency is highest for the x = 0.60 cell at 13.8%, and all the compositions have efficiency comparable to the Cu:ZnTe baseline efficiency of 14.0%.

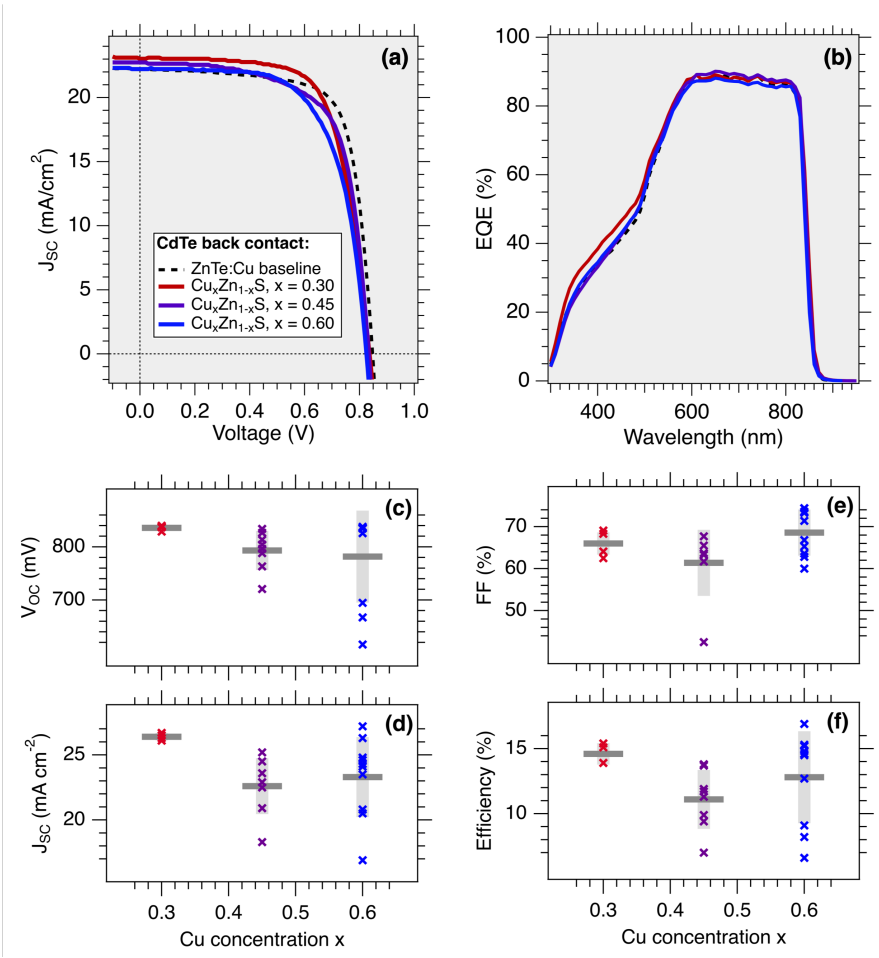

Figure 3: (a) JV and (b) EQE measurements of different stoichiometries of $Cu_xZn_{1-x}S$ films as back contacts to CdTe for highest performing cells. Control devices using ZnTe:Cu are plotted for comparison. The distribution of (c) open-circuit voltage (V_{OC}), (d) short-circuit current (J_{SC}), (e) fill factor (FF), and (f) efficiency (η) values are plotted across all measured cells in this study. Note that (a) is corrected from EQE measurements, but (d) and (f) are not.

Statistically, the solar cell parameters are least variant across the x = 0.30 cells, where the average efficiency is the highest, and the highest EQE-corrected efficiency is achieved for x = 0.60. However, overall the efficiencies of all three samples are very similar, within a percent or so and all within statistical uncertainty of one another. It may be of interest that the x = 0.30 data are the least scattered, and that the scatter and average V_{OC} increase with increasing x where materials are expected from XRD to phase-segregate,[43] though we note there are fewer cells measured for x = 0.30. Statistical analysis across all solar cells

Table 1: The best achieved CdTe solar cell parameters for a given contact material

Back contact to CdTe	$\mathbf{V_{OC}}$ **(mV)**	$\mathbf{J_{SC}}$ **(mA/cm²)**	$\mathbf{J_{SC}}^{\textbf{from EQE}}$ **(mA/cm²)**	**FF (%)**	η **(%)**	$\eta^{\textbf{from EQE}}$ **(%)**	$\mathbf{R_s}$ **(Ω cm²)**	$\mathbf{R_{sh}}$ **(Ω cm²)**
$Cu_{0.30}Zn_{0.70}S$	837	26.7	23.03	69.1	15.4	13.3	4.3	2,600
$Cu_{0.45}Zn_{0.55}S$	834	24.5	22.74	67.7	13.8	12.8	3.1	2,200
$Cu_{0.60}Zn_{0.40}S$	836	24.6	22.22	74.4	15.3	13.8	3.9	1,700
Cu:ZnTe baseline	848	26.6	22.40	73.3	16.6	14.0	2.6	1,200

measured is elaborated upon in the Supporting Information.

External quantum efficiency (EQE) measurements of the same highest performing cells are plotted in Figure 3(b), revealing EQEs equal to or greater than the optimized baseline back contact cells. We comment that EQE differences at low wavelengths are likely from parasitic absorption at the Cd(O,S) front buffer layer, as reported elsewhere,[58] rather than from the back contact region. Shunt resistances (R_{sh}) and series resistances (R_s) are estimated from the slopes at the J_{SC} and V_{SC}, respectively. R_{sh} >1,000 Ω cm^2 and fill factors of nearly 75% for $Cu_xZn_{1-x}S$ contacts with little optimization to date is very encouraging. R_s is low, but can be addressed by further optimizing composition, thickness, and material quality of the $Cu_xZn_{1-x}S$ layer using insights from this study. It is also important to note that grain size of the contact layer may influence the V_{OC}, J_{SC}, and resistances in these devices, as absorber and contact grain size has been shown to influence performance in the literature.[59,60] However, our previous study of $Cu_xZn_{1-x}S$ suggests a grain size of approximately 10˘50 nm to be relatively constant in the range $0.3 < x < 0.9$, so here grain size is unlikely to have a significant impact.[43]

Device Stability in Air

Next, **Figure 4** illustrates the stability of the three highest performing cells over one year (approximately 9,000 hours) in air. Assessing stability is particularly important in chalcogenide-based devices, since chalcogenide materials are known to experience enhanced degradation pathways due to oxidation. Additionally, the presence of highly-diffusive Cu^{+1} ions has been

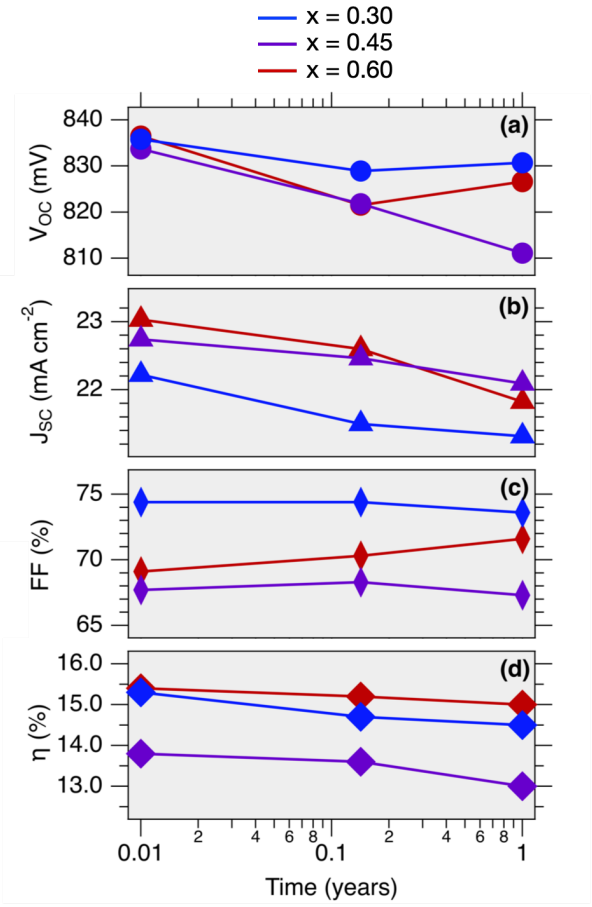

Figure 4: Stability of (a) open-circuit voltage (V_{OC}), (b) short-circuit current (J_{SC}), (c) fill factor (FF), and (d) efficiency (η) as a function of time for $Cu_xZn_{1-x}S$ back contact CdTe devices stored in air. Note that (a) values are corrected from EQE measurements.

shown to contribute detrimentally to CdTe device stability by inducing spurious rectification.[16,61] Figure 4 plots the stability of the (a) V_{OC}, (b) J_{SC} (corrected from EQE), (c) FF, and (d) efficiency (η) as a function of time over the course of a year for the three devices investigated in this study. With a few exceptions including the dip at 20 days after fabrication (0.055 years), possibly due to fluctuations in the light source, device properties generally decrease monotonically and only negligibly over the course of a year. V_{OC} decreases by 1–3% and efficiency decreases by 3–6%. Unfortunately, the control cell was damaged shortly after the first measurement, so could not be compared for this analysis but should be included in follow-up work. Such a shelf-life stability test shows that Cu diffusion at room temperature is not prohibitively bad, but long-term degradation studies under illumination

at maximum power point, continuous operation, and elevated temperatures are warranted in the future. First Solar modules with optimized ZnTe are warranted to have 0.5%/yr (relative) degradation or less in the field,[62] so competitor contacts would have to hold up to this metric.

Contact Barrier Height and Carrier Lifetime Measurements

As described previously, back contact interfacial resistance can lead to a significant deviation from ideality in CdTe solar cells, and an optimal contact has a small or negligible Schottky barrier. To assess this barrier height Φ_b, we measured dark JV curves at a variety of sub-ambient temperatures, as described in the literature.[63,64] The "turning current" J_t, at which a JV curve transitions from a positive to negative second derivative, is fit for each temperature (c.f. Supporting Information for details) as shown in **Figure 5**(a). Then the Richardson equation[65] is used to calculate barrier height,

$$J_t = A^* T^2 e^{-q\Phi_b/kT} \tag{1}$$

where A^* is the Richardson constant and k is the Boltzmann constant. We find Φ_b values for x = 0.30, 0.45, and 0.60 of 298 ± 13 meV, 304 ± 11 meV, and 316 ± 13 meV, respectively, and plot each in Figure 5(b). As depicted in Figure 5(b), typical CdTe barrier heights using standard back contacts are approximately 300−500 meV. Thus, these values are in the range considered small for CdTe devices, which is consistent with the shapes of the JV curves and the JV parameters achieved. A slight increase in barrier height with x, coupled with the slight increase in conductivity with x observed in Figure 2(b), may explain why the solar cell performance dips at the mid-range of x = 0.45 (see Figure 3, though this is mere speculation and there could be many simultaneous effects occurring.

Contacts must effectively passivate the CdTe absorber such that recombination is minimal. Thus, characterizing the minority carrier recombination lifetime of these devices can

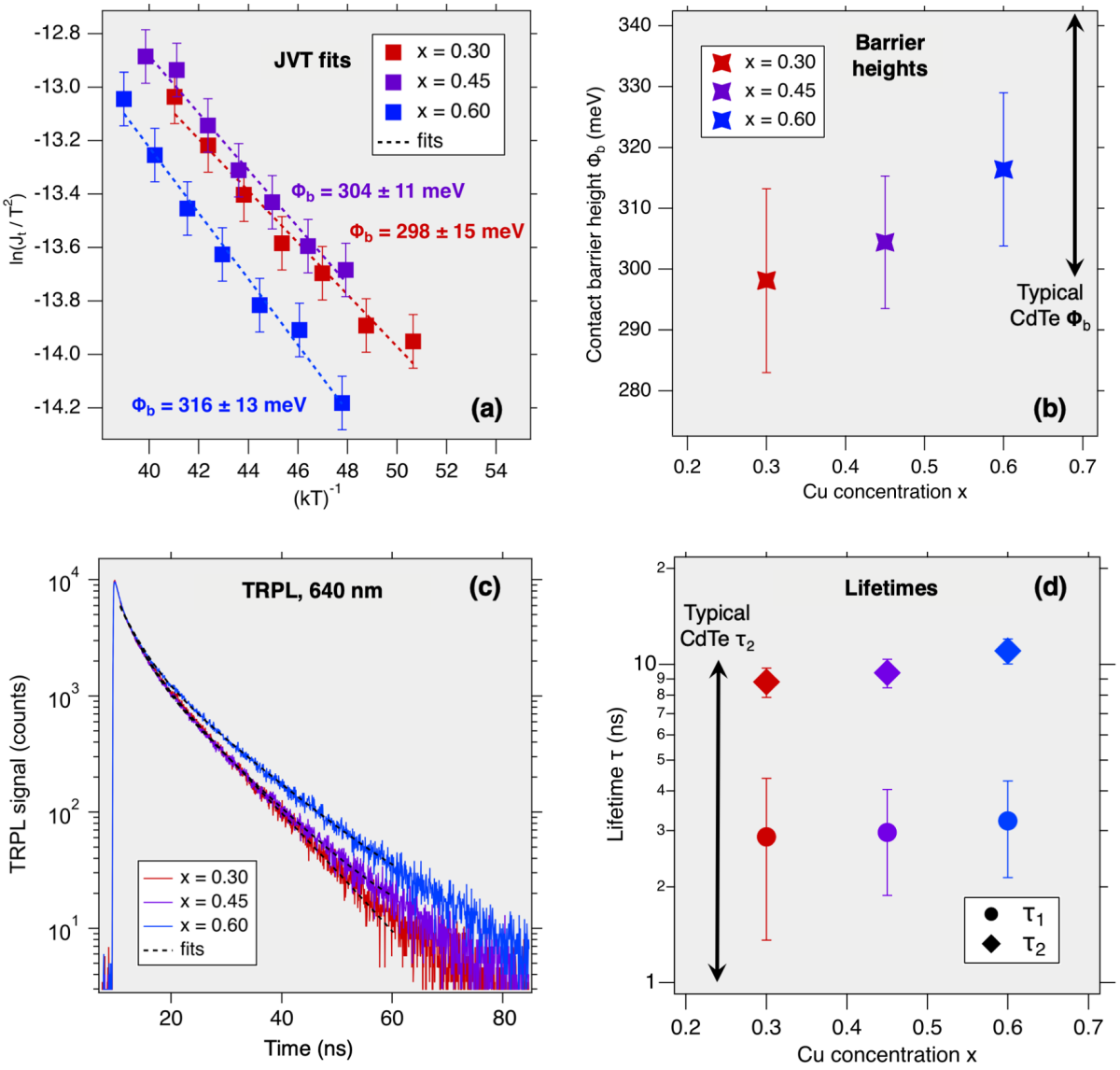

Figure 5: (a) Linear fits to temperature dependent JV (JVT) measurements, as described in the Supporting Information, and (b) back contact barrier heights as quantified by (a) in the three devices of interest, with the typical CdTe range boxed. (c) Time-resolved photoluminescence (TRPL) of the three highest performing $Cu_xZn_{1-x}S$ back contact devices in this study, with bi-exponential decay fits plotted, and (d) resulting carrier lifetimes from fits to these measurements. Parameters τ_1 and τ_2 correspond to the former and latter sections of the decay curve, respectively, and error bars are from uncertainty in fit.

help assess whether the absorber layer has been compromised due to the addition of the new back contact. As described in the Introduction, Cu can be detrimental because of its tendency to diffuse into the absorber and induce compensation, and has been shown to influence lifetime.[21,66,67] Shown in Figure 5(c) and (d), time-resolved photoluminescence (TRPL) measurements on our three devices indicate τ_2 = 9–10 ns and τ_1 =$\sim$3 ns, respectively. Lifetime τ_2 is generally on the order of several ns (depicted with an arrow in Figure 5(d)) whereas τ_1 is typically about 0.5–1.5 ns, assuming $CdCl_2$ treatment. As-deposited the lifetimes are on the order of tens to hundreds of picoseconds. We can assert that our values are typical for CdTe solar cells and thus, $Cu_xZn_{1-x}S$ back contacts demonstrate no significant degradation of the CdTe absorber.

Imaging the Interface

The above results beget the following questions: what is the nature of the CdTe$-Cu_xZn_{1-x}S$ interface, why is there a larger statistical distribution of solar cell parameters with increasing x, and from which mechanism does observed degradation originate? To assess these, we first investigate the interfacial back contact regions of each device stack using cross-sectional scanning electron microscopy (SEM) after a year of aging in air. Images in **Figure 6** denote the as-deposited CdTe, $Cu_xZn_{1-x}S$, and Au regions, with the Au surface visible at the top of the figure. We observe the $Cu_xZn_{1-x}S$ layer to be conformal on the surface of polycrystalline CdTe in all three images, with columnar grains. These images confirm $Cu_xZn_{1-x}S$ thicknesses between 200 nm and 300 nm. What is surprising is that there appears to be an additional interfacial layer forming, indicated by the darker region between $Cu_xZn_{1-x}S$ and CdTe. This interfacial effect appears in all samples, increasing in thickness as x increases. The dark region appears to extend into the grains of the CdTe layer rather than the $Cu_xZn_{1-x}S$ layer. We also observe a few dark spots in the x = 0.30 sample between the $Cu_xZn_{1-x}S$ and CdTe.

To further understand interfacial chemistry and identify the dark interfacial region observed in SEM, we performed cross-sectional scanning transmission electron microscopy

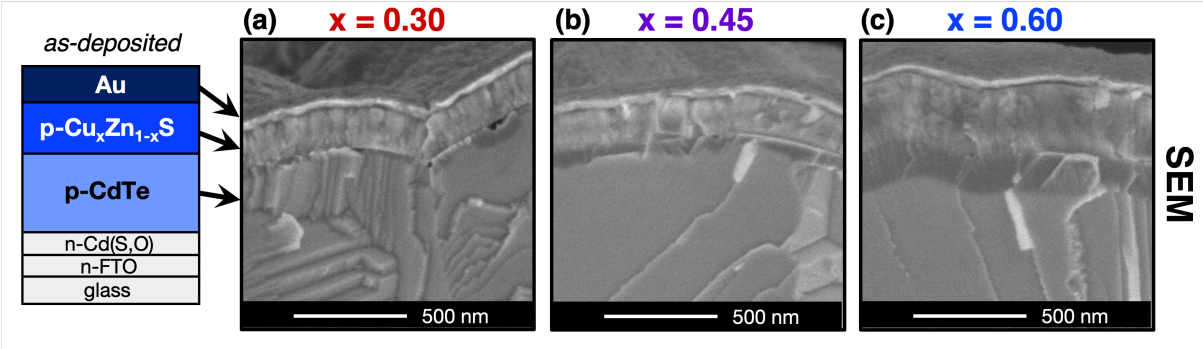

Figure 6: Scanning electron microscopy (SEM) images of the $Cu_xZn_{1-x}S$ back-contact interfacial region for devices with (a) x = 0.30, (b) x = 0.45, and (c) x = 0.60. As-deposited schematic layers from Figure 1 are illustrated on the left for clarification.

(STEM) on the CdTe–$Cu_xZn_{1-x}S$–Au interface prepared by FIB lift-out on Mo TEM grids for an x = 0.30 and an x = 0.60 sample after a year of aging. These samples are selected because they possess the thinnest and thickest dark interfacial regions and highest cell performances. The interfaces are shown as STEM high-angle annular dark-field (HAADF) images in **Figures 7**(a) and (b), respectively, with stoichiometry determined by an energy-dispersive X-ray spectroscopy (EDS) line scan (red horizontal arrows) in (c) and (d), respectively. The images are aligned with the x axis of the scans, and we note different scaling in the two samples. Regions are labeled to contain a particular element if the concentration is greater than 10%, otherwise the element is notated as "trace." Quantified EDS results are included in the Supporting Information, and we note EDS concentration is in atomic percent and a detection limit of approximately 1%.

These measurements show that the dark interfacial regions are phase segregated bilayers, and the identities of these regions are revealed as follows (going left to right across each image in Figure 7). For the x = 0.30 interface, the CdTe region contains approximately 10% excess Cu, and then the Te concentration spikes at the interface. This thin (approx. 45 nm) Te-rich region contains Cu and S, so it is labeled "Cu-Te-S," and has trace amounts of Zn and Cd. Cu-rich inclusions were observed in some regions of the CdTe–Cu-Te-S interface (c.f. Supporting Information). Next, a 175 nm layer of primarily Zn and S emerges, with

~10% Cd and just under ~10% Cu (labeled "Zn-Cd-Cu-S"). This layer gradually transitions through the interlayer (labeled "IL") into the Au contact region ("Cu-Au-S"), in which we observe a higher elemental concentration of Cu than of Au, as well as approx. 18% S (though this may be an analysis artifact from overlapping S K and Au M peak). In the x = 0.60 sample, first we observe that the CdTe region is somewhat Cd-poor and contains trace O and S. Next, in place of the as-deposited $Cu_{0.60}Zn_{0.40}S$ layer, we observe a bilayer containing (1) a 150 nm thick Cu-Te-S layer in contact with CdTe, which is the dark interfacial region from the SEM, and (2) a 300 nm thick Cd-Zn-S layer (with trace Cu), located between Cu-Te-S and Au. Then the Au contact contains approximately 25% S (potentially an artifact, see above) as well as trace Cu and Zn. The far right region in both images is a Pt protective layer from the FIB sample preparation process.

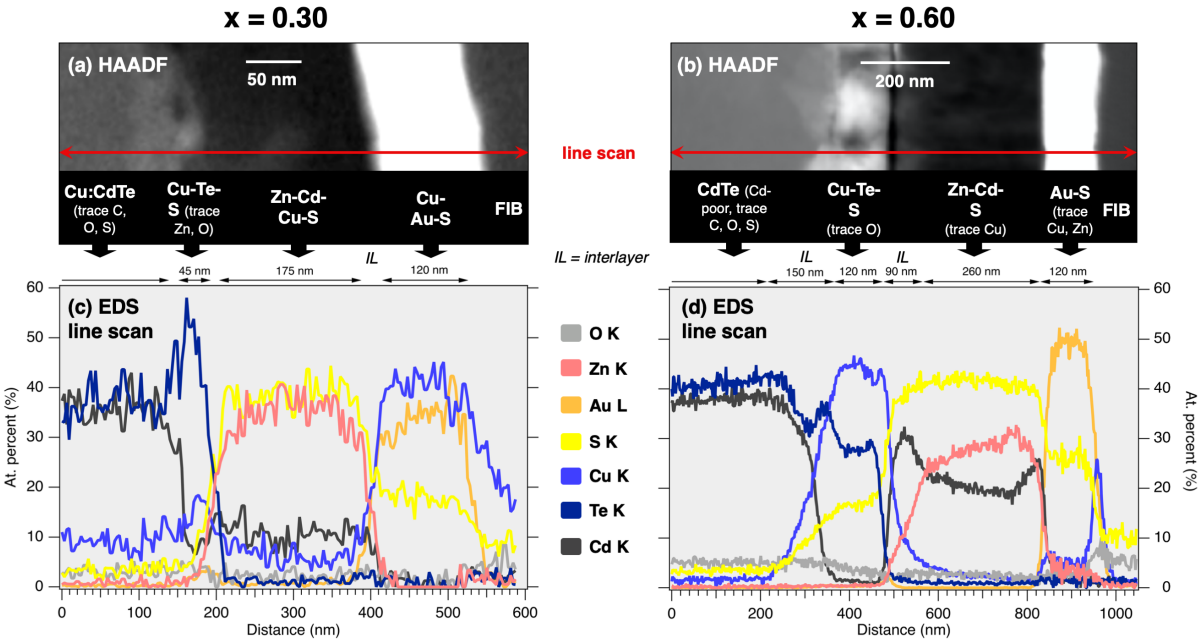

Figure 7: Cross-sectional scanning transmission electron microscopy (STEM) HAADF images of the CdTe−$Cu_xZn_{1-x}S$−Au interfacial region of representative (a) x = 0.30 and (b) x = 0.60 cells, with elemental energy-dispersive X-ray spectroscopy (EDS) line scans for the (c) x = 0.30 and (d) x = 0.60 cells. The red lines in (a) and (b) indicate the region through which the EDS line scan was measured. "IL" indicates interlayer regions. Elemental profiles in (c) and (d) are indicated by trace color. These images reveal complex interfacial chemistry, with a bilayer in place of the $Cu_xZn_{1-x}S$ as-deposited layer and diffusion profiles of various elements.

Since STEM was performed after aging cells for one year, it is unclear from this investigation whether the bilayer formation is induced by aging in air at room temperature, from the anneal step during cell fabrication, or from some other energetic transition. It is also unclear whether the segregation is the cause of the slight degradation in cell performance. We acknowledge that there is concern for additional ion migration and additional shunt resistance under operation and upon exposure to high temperature and UV radiation; this has not been explicitly studied here, and certainly warrants future investigation. However, it is significant that in all cells this phase-segregated bilayer interfacial configuration still leads to good carrier lifetimes, sufficient hole transport, and PV performance equivalent to the control samples.

Chemical Stability Analysis

From the STEM–EDS analysis, it is unclear whether these bilayer phases are alloys or composites, since the crystal structure of each phase is not determined. There is evidence in the literature of a ternary S-rich $Cu_{10}Te_4S_{13}$ phase,[68] though the Cu-Te-S layers are Te-rich. We observe inversely correlated Cu and Te fluctuations in the Cu-Te-S layer on the order of 50 to 100 nm. This suggests phase segregation and perhaps a Cu_xTe:Cu_yS composite with fluctuating Cu concentration x (c.f. Supporting Information). Both of these binaries are p-type semiconductors. The Zn-Cd-S layer contains inverted fluctuations of Zn and Cd, suggesting a phase segregation into Zn-rich and Cd-rich ternary phases, with smaller phase coherence on the order of 40 to 80 nm. These layers could be an n-type wurtzite $Cd_xZn_{1-x}S$ solid solution or a composite, both of which have been synthesized extensively in the literature.[69,70]

We calculate thermochemical stability of the as-deposited interface from first principles to help understand our resulting bilayer. Using the Interfacial Reaction Calculator from the Materials Project,[47,48] we investigate the reactions and resulting phases expected to occur at a $Cu_xZn_{1-x}S$−CdTe interface for x = 0.30, 0.45, and 0.60, at lowest formation enthalpy (δH), and report reactions and their associated reaction energies (E_{rxn}) in **Table**

2. We note that this calculator is based on convex hull analysis such that reactants are phase segregated Cu_yS:ZnS, and only shows reaction products with a convex hull energy of 0 eV/atom (i.e. only thermodynamically stable phases), though metastable phases may actually form experimentally. We calculate products of ZnS, CdS, and CuTe, with negative E_{rxn} values of -1.898, -2.553 and -3.085 kJ/mol for x = 0.30, 0.45, and 0.60, respectively. From these calculations, and negative E_{rxn} values, we hypothesize that a zinc blende or wurtzite ZnS phase, wurtzite CdS phase ($P6_3mc$, mp-672), and layered CuTe phase ($Pmmn$, mp-20826) are favorable to form under canonical thermodynamic conditions. Indeed, the STEM results are suggestive of a similar phase separation behavior. The CdS and ZnS products coexist in a single layer. CuTe also separates into its own layer, with some residual S present. The lower E_{rxn} in the x = 0.60 sample may explain why the dark phase segregated Cu-Te-S layer is more prominent in the SEM images of Figure 6, and why the bilayers observed by STEM are thicker. Since x = 0.45 has a E_{rxn} between that of x = 0.30 and x = 0.60, we could expect a similar phase segregation to occur, likely with a Cu-Te-S layer thickness larger than 45 nm and smaller than 120 nm.

For comparison we calculate equilibrium reactions of $Cu_xZn_{1-x}Te$–CdTe (standard back contact) to yield an additional CuTe product (see Supporting Information). It has been shown that in CdTe cells with a Cu:ZnTe buffer layer, the activation (i.e. annealing) step induces a bilayer structure at the CdTe−CuZnTe interface with a disordered layer due to Cd-Zn interdiffusion and a Cu_xTe phase segregated layer at defects,[71] supported by our reaction calculations. Thus it is reasonable that a similar effect is occurring at the CdTe−$Cu_xZn_{1-x}S$ interface, because nearly all of the same elements are participating. For reference, in the Supporting Information we also report thermodynamic stability calculations of CdTe interfaces for other back contacts in the literature, demonstrating stable interfaces for Sb_2Te_3 and As_2Te_3 and unstable interfaces for Cu_xS, CuI, CuCSN, NiO_x, and MoO_x, though we acknowledge the simplicity of our assumptions.

Table 2: Lowest enthalpy interfacial reactions under thermodynamic equilibrium, assuming a closed reaction, at three $Cu_xZn_{1-x}S$ interfaces with CdTe.

Interface with CdTe	**Interfacial reaction equation (normalized)**	**E_{rxn} of eqn (kJ/mol)**
$Cu_{0.3}Zn_{0.7}S$	0.769 $Cu_{0.3}Zn_{0.7}S$ + 0.231 CdTe → 0.538 ZnS + 0.231 CdS + 0.231 CuTe	-1.898
$Cu_{0.45}Zn_{0.55}S$	0.69 $Cu_{0.45}Zn_{0.55}S$ + 0.31 CdTe → 0.379 ZnS + 0.31 CdS + 0.31 CuTe	-2.553
$Cu_{0.6}Zn_{0.4}S$	0.625 $Cu_{0.6}Zn_{0.4}S$ + 0.375 CdTe → 0.25 ZnS + 0.375 CdS + 0.375 CuTe	-3.085

Implications

Here, we discuss the extent to which our experimental results correspond to the design criteria (1)-(6) outlined in the Introduction. We confirmed with Hall measurements that $Cu_xZn_{1-x}S$ is p-type doped (Condition 1), but the doping of each of the bilayers, their E_F position (Condition 3), and the band bending at the interface are unclear from this analysis. We have measured a back contact valence band barrier height of approximately 0.3 eV from JVT, which is relatively low for CdTe and allows transport of holes with minimal losses (Condition 2). However, because we observe a bilayer back contact, this could be a compounded barrier height from both layers and thus is difficult to interpret directly. Band offsets would need to be probed experimentally to confirm the exact VB offset, and whether the contact is actually electron reflecting (Condition 4). Counter to the expected criteria (Condition 5), we demonstrate with STEM and thermochemistry calculations that the back contact interface is *not* chemically stable, at least not initially, though only slight degradation in cell performance after a year suggests it may stabilize after operation. From τ_2 lifetimes of 9–10 ns, we can claim that even though it contains Cu the contact does not destroy the CdTe absorber, but we cannot claim passivation without further analysis (Condition 6). Additionally processing was carried out at temperatures below 200 °C, which is considered a low enough thermal budget to minimize damage to the absorber, though it is unclear from this study whether the interfacial instabilities occur immediately after processing or after operation.

Previous study assumes that the $Cu_xZn_{1-x}S$ back contact remains in its as-deposited com-

posite form,[44] but this paper shows that is actually not the case, contributing to knowledge in the field. Rather than a $Cu_xZn_{1-x}S$ back contact, we instead have observed effectively a mixed-phase Cu-Te-S contact, and a Zn-Cd-S buffer layer. This interfacial complexity is not uncommon in device applications — as previously mentioned, current CdTe contact materials like Cu:ZnTe have also been shown to form more complexity at the interfaces than assumed.[71] In our study, the thickness of the Cu-Te-S layer appears to increase with as-deposited Cu concentration x, correlating with an increase in barrier height Φ_b and slight decrease in solar cell performance and increase in statistical scatter of J_{SC}, V_{OC}, fill factor, and efficiency. Both Cu-Te and Cu-S have been explored as hole selective back contacts to CdTe for decades;[20–23] for example, optimized single-phase Cu_xTe back contacts with rapid thermal processing have yielded efficiencies up to 13.9% and have been reported to minimize back contact recombination,[22] and Cu_xS back contacts have recently reported efficiencies up to 13%, though VBM offsets are slightly too high at 0.4−0.6 eV.[25] $Cd_xZn_{1-x}S$ has also been used as a contact with CdTe, but as an electron selective *front* contact rather than a back contact. The charge transport mechanism at this bilayer interface is particularly elusive since $Cd_xZn_{1-x}S$ is usually a n-type semiconductor. However, Zn-Cd-S carrier concentrations here are unknown, and the Zn-Cd-S region could be p-type e.g. due to Cu substitutions. We still do not know the band alignment of the bilayer; understanding this will require future investigation. For insight into the charge transport through our bilayer, we can look towards other literature reports of bilayer back contacts.

A recent report investigated an intentional bilayer, ZnTe and Cu_xTe (x = 1.4) as a back contact to CdTe solar cells, resulting in high fill factors >73%.[72] In our study, the Cu_xTe component of the bilayer is in contact with Au, rather than with CdTe, yet still achieves similar solar cell properties to this study, suggesting pathways to further optimization. Other bilayer CdTe back contacts have been reported elsewhere in the literature, e.g. p-type SrCuSeF−n-type In_2O_3:Sn bilayer Ohmic tunnel junctions have demonstrated higher efficiencies together than each material as a single back contact.[73] Quasi-Ohmic tunnel junc-

tions are used to convert carrier type from electrons such that n-type layers can transport holes.[74] Bilayer and even tri-layer carrier selective contacts are used extensively for other photovoltaic device applications, e.g. p-type a-Si−n-type TCO hole selective contacts in silicon heterojunction solar cells,[75–77] such that one material does not need to satisfy all requirements. In this study, formation of a stable bilayer back contact with good photovoltaic performance may suggest a promising design route for CdTe back contact exploration.

Conclusion

We have investigated the use of sputtered $Cu_xZn_{1-x}S$ (x = 0.30, 0.45, 0.60) as a hole selective back contact for polycrystalline CdTe solar cells. We demonstrate separation into a bilayer of Cu-Te-S and Zn-Cd-S at the back interface for x = 0.30 and x = 0.60 cells, that still yield device performance nearly as high as cells with standard control back contacts. Specifically, we report a fill factor of 74.4% without optimization. Relatively low contact barrier heights of approximately 300 meV suggest small losses due to charge transport. V_{OC} measurements of 837 mV and high τ_2 lifetime measurements of approximately 9–10 ns suggest the back contact is not degrading either the absorber or front interface through Cu diffusion or other mechanisms. Efficiency was similar to control devices. After one year aged in air, V_{OC} is reduced by only 1–3% and efficiencies by 3–6%. Although these samples use CdS buffers and the JV parameters are far from the best polycrystalline CdTe devices in the literature, it significant that these results are achieved with no device optimization, suggesting optimization may yield further improvement.

This investigation motivates follow-up research on incorporation of $Cu_xZn_{1-x}S$ as a back contact for CdTe solar cells, and on the bilayer contact formation. First, a more in-depth exploration of $Cu_xZn_{1-x}S$ thickness, Cu concentration, deposition temperature, and synthesis method should be pursued to investigate whether the ternary can be thermochemically stabilized. Alloying in the Zn(S,Se,Te) phase space could also be explored as a possibility

to tune barrier height and increase passivation. Second, device modeling and experimental analysis using x-ray photoelectron spectroscopy (XPS) can be performed to assess band edges, determine interfacial band-bending, and inform optimal growth conditions. Third, further interfacial characterization is recommended to understand the role of diffusion, the physics of the interfacial layer(s), grain boundary segregation, hole transport at the interface, etc. Stress testing and temperature dependent performance should be assessed. It is also of interest to investigate whether the interfacial bilayer indeed forms at different Cu concentrations, and to intentionally grow a bilayer back contact.

More broadly, since such high performance is achieved upon first try, this study should also inspire research to incorporate underexplored semi-transparent p-type materials as back contacts, such as those outlined in our most recent review article,[18] in both single-layer and bilayer configurations. Many new compounds are becoming available to the scientific community as a result of high-throughput computational and experimental searches for wide gap p-type semiconductors. In particular, the use of combinatorial synthesis coupled to device optimization has been demonstrated as a promising avenue to rapidly explore phase space and optimize such new contact materials.[78] Perhaps the incorporation of one of these underexplored materials such as $Cu_xZn_{1-x}S$ in a well-optimized configuration will enable elimination of voltage losses at the back interface and push CdTe solar cell efficiencies towards their 30% theoretical detailed balance limit.

Acknowledgments

This work was authored at the National Renewable Energy Laboratory, operated by Alliance for Sustainable Energy, LLC, for the U.S. Department of Energy (DOE) under Contract No. DEAC36-08GO28308. Funding is provided by the Office of Science (SC), Office of Basic Energy Sciences (BES), as part of the Energy Frontier Research Center "Center for Next Generation of Materials Design: Incorporating Metastability." R.W.R. acknowledges her Ph.D.

funding from the U.C. Berkeley Chancellor's Fellowship and the National Science Foundation (NSF) Graduate Research Fellowship Program (GRFP) under Grant Numbers DGE1106400 and DGE1752814. The use of thin film synthesis and spatially-resolved characterization facilities at NREL, as a part of High Throughput Experimental Materials Collaboratory (HTE-MC), is acknowledged. The authors gratefully acknowledge Dr. Bobby To for SEM measurements, and Dr. David Albin, Dr. Shyam Dwaraknath, Dr. Angela Fioretti, Dr. Yanbing Han, and Dr. Matthew Horton for fruitful discussion. The views expressed in the article do not necessarily represent the views of the DOE or the U.S. Government.

Supporting Information

The following supporting information is included:

- S1 Materials Properties
- S2 Device Properties
- S3 Interfacial Reaction Calculations
- S4 Experimental Details

References

(1) Green, M. A.; Hishikawa, Y.; Dunlop, E. D.; Levi, D. H.; Hohl-Ebinger, J.; Ho-Baillie, A. W. Solar cell efficiency tables (version 52). *Progress in Photovoltaics: Research and Applications* **2018**, *26*, 427–436.

(2) Munshi, A. H.; Sasidharan, N.; Pinkayan, S.; Barth, K. L.; Sampath, W.; Ongsakul, W. Thin-film CdTe photovoltaics–The technology for utility scale sustainable energy generation. *Solar Energy* **2018**, *173*, 511–516.

(3) Shockley, W.; Queisser, H. J. Detailed balance limit of efficiency of p-n junction solar cells. *Journal of applied physics* **1961**, *32*, 510–519.

(4) Geisthardt, R. M.; Topič, M.; Sites, J. R. Status and potential of CdTe solar-cell efficiency. *IEEE Journal of photovoltaics* **2015**, *5*, 1217–1221.

(5) Duenow, J. N.; Metzger, W. K. Back-surface recombination, electron reflectors, and paths to 28% efficiency for thin-film photovoltaics: A CdTe case study. *Journal of Applied Physics* **2019**, *125*, 053101.

(6) Fritsche, J.; Gunst, S.; Thiβen, A.; Gegenwart, R.; Klein, A.; Jaegermann, W. CdTe thin film solar cells: the CdS/SnO_2 front contact. *MRS Online Proceedings Library Archive* **2001**, *668*.

(7) Abbas, A.; Meysing, D. M.; Reese, M.; Barnes, T. M.; Walls, J.; Wolden, C. A. Structural and chemical evolution of the CdS: O window layer during individual CdTe solar cell processing steps. *Solar Energy* **2018**, *159*, 940–946.

(8) Kephart, J.; McCamy, J.; Ma, Z.; Ganjoo, A.; Alamgir, F.; Sampath, W. Band alignment of front contact layers for high-efficiency CdTe solar cells. *Solar Energy Materials and Solar Cells* **2016**, *157*, 266–275.

(9) Ablekim, T.; Perkins, C.; Zheng, X.; Reich, C.; Swanson, D.; Colegrove, E.; Duenow, J. N.; Albin, D.; Nanayakkara, S.; Reese, M. O.; Shimpi, T.; Sampath, W.; Metzger, W. K. Tailoring MgZnO/CdSeTe Interfaces for Photovoltaics. *IEEE Journal of Photovoltaics* **2019**, *9*, 888–892.

(10) Gessert, T.; Mason, A.; Sheldon, P.; Swartzlander, A.; Niles, D.; Coutts, T. Development of Cu-doped ZnTe as a back-contact interface layer for thin-film CdS/CdTe solar cells. *Journal of Vacuum Science & Technology A: Vacuum, Surfaces, and Films* **1996**, *14*, 806–812.

(11) Tang, J.; Mao, D.; Ohno, T.; Kaydanov, V.; Trefny, J. Properties of ZnTe: Cu thin films and CdS/CdTe/ZnTe solar cells. Conference Record of the Twenty Sixth IEEE Photovoltaic Specialists Conference-1997. 1997; pp 439–442.

(12) Li, J.; Diercks, D. R.; Ohno, T. R.; Warren, C. W.; Lonergan, M. C.; Beach, J. D.; Wolden, C. A. Controlled activation of ZnTe: Cu contacted CdTe solar cells using rapid thermal processing. *Solar Energy Materials and Solar Cells* **2015**, *133*, 208–215.

(13) Reese, M. O.; Perkins, C. L.; Burst, J. M.; Farrell, S.; Barnes, T. M.; Johnston, S. W.; Kuciauskas, D.; Gessert, T. A.; Metzger, W. K. Intrinsic surface passivation of CdTe. *Journal of Applied Physics* **2015**, *118*, 155305.

(14) Li, J. V.; Duenow, J. N.; Kuciauskas, D.; Kanevce, A.; Dhere, R. G.; Young, M. R.; Levi, D. H. Electrical characterization of Cu composition effects in CdS/CdTe thin-film solar cells with a ZnTe: Cu back contact. 2012 IEEE 38th Photovoltaic Specialists Conference (PVSC) PART 2. 2012; pp 1–5.

(15) Alfadhili, F. K.; Phillips, A. B.; Liyanage, G. K.; Gibbs, J. M.; Jamarkattel, M. K.; Heben, M. J. Controlling Band Alignment at the Back Interface of Cadmium Telluride Solar Cells using ZnTe and Te Buffer Layers. *MRS Advances* **2019**, *4*, 913–919.

(16) Demtsu, S.; Sites, J. Effect of back-contact barrier on thin-film CdTe solar cells. *Thin Solid Films* **2006**, *510*, 320–324.

(17) Mathew, X.; Thompson, G. W.; Singh, V.; McClure, J.; Velumani, S.; Mathews, N.; Sebastian, P. Development of CdTe thin films on flexible substrates—a review. *Solar Energy Materials and Solar Cells* **2003**, *76*, 293–303.

(18) Woods-Robinson, R.; Han, Y.; Zhang, H.; Ablekim, T.; Khan, I.; Persson, K. A.; Zakutayev, A. Wide band gap chalcogenide semiconductors. *Chemical Reviews* **2020**,

(19) Liyanage, G. K.; Phillips, A. B.; Alfadhili, F. K.; Ellingson, R. J.; Heben, M. J. The Role of Back Buffer Layers and Absorber Properties for$>$ 25% Efficient CdTe Solar Cells. *ACS Applied Energy Materials* **2019**, *2*, 5419–5426.

(20) Ferekides, C.; Viswanathan, V.; Morel, D. RF sputtered back contacts for CdTe/CdS thin film solar cells. Conference Record of the Twenty Sixth IEEE Photovoltaic Specialists Conference-1997. 1997; pp 423–426.

(21) Wu, X.; Zhou, J.; Duda, A.; Yan, Y.; Teeter, G.; Asher, S.; Metzger, W.; Demtsu, S.; Wei, S.-H.; Noufi, R. Phase control of Cu_xTe film and its effects on CdS/CdTe solar cell. *Thin Solid Films* **2007**, *515*, 5798–5803.

(22) Yang, Y.; Wang, T.; Liu, C.; Li, W.; Zhang, J.; Wu, L.; Zeng, G.; Wang, W.; Yu, M. Single-phase control of CuTe thin films for CdTe solar cells. *Vacuum* **2017**, *142*, 181–185.

(23) Kim, D.; McCandless, B.; Hegedus, S.; Birkmire, R. Cu_xS back contact for CdTe solar cells. *Proceedings of 3rd World Conference on Photovoltaic Energy Conversion, 2003* **2003**, *1*, 360–363.

(24) Donghwan, K.; McCandless, B.; Hegedus, S.; Birkmire, R. Cu_xS back contact for CdTe solar cells. *Revista mexicana de física* **2007**, *53*, 5–8.

(25) Türck, J.; Siol, S.; Mayer, T.; Klein, A.; Jaegermann, W. Cu_2S as ohmic back contact for CdTe solar cells. *Thin Solid Films* **2015**, *582*, 336–339.

(26) Rose, D. H.; Hasoon, F. S.; Dhere, R. G.; Albin, D. S.; Ribelin, R. M.; Li, X. S.; Mahathongdy, Y.; Gessert, T. A.; Sheldon, P. Fabrication procedures and process sensitivities for CdS/CdTe solar cells. *Progress in Photovoltaics: Research and Applications* **1999**, *7*, 331–340.

(27) Li, X.; Xiao, D.; Wu, L.; Wang, D.; Wang, G.; Wang, D. CdTe thin film solar cells with copper iodide as a back contact buffer layer. *Solar Energy* **2019**, *185*, 324–332.

(28) Montgomery, A.; Guo, L.; Grice, C.; Awni, R. A.; Saurav, S.; Li, L.; Yan, Y.; Yan, F. Solution-processed copper (I) thiocyanate (CuSCN) for highly efficient CdSe/CdTe thin-film solar cells. *Progress in Photovoltaics: Research and Applications* **2019**, *27*, 665–672.

(29) Liang, J.; Bi, H.; Wan, D.; Huang, F. Novel Cu nanowires/graphene as the back contact for CdTe solar cells. *Advanced Functional Materials* **2012**, *22*, 1267–1271.

(30) Schmidt, T.; Durose, K.; Rothenhäusler, C.; Lerch, M. Chemical stability of Sb_2Te_3 back contacts to CdS/CdTe solar cells. *Thin Solid Films* **2000**, *361*, 383–387.

(31) Abken, A.; Bartelt, O. Sputtered Mo/Sb_2Te_3 and Ni/Sb_2Te_3 layers as back contacts for CdTe/CdS solar cells. *Thin Solid Films* **2002**, *403*, 216–222.

(32) Hu, S.; Zhu, Z.; Li, W.; Feng, L.; Wu, L.; Zhang, J.; Gao, J. Band diagrams and performance of CdTe solar cells with a Sb_2Te_3 back contact buffer layer. *AIP Advances* **2011**, *1*, 042152.

(33) Romeo, N.; Bosio, A.; Mazzamuto, S.; Romeo, A.; Vaillant-Roca, L. High efficiency CdTe/CdS thin film solar cells with a novel back contact. *Proceedings of the 22nd European Photovoltaic Solar Energy Conference* **2007**, 1919–1927.

(34) Rockett, A.; Marsillac, S.; Collins, R. Novel contact materials for improved performance CdTe solar cells final report. *Colorado School of Mines, Golden, CO (United States)* **2018**,

(35) Lin, H.; Xia, W.; Wu, H. N.; Gao, Y.; Tang, C. W. MoO_x back contact for CdS/CdTe thin film solar cells: Preparation, device characteristics, and stability. *Solar Energy Materials and Solar Cells* **2012**, *99*, 349–355.

(36) Paudel, N.; Compaan, A.; Yan, Y. Sputtered CdS/CdTe solar cells with MoO_{3-x}/Au back contacts. *Solar Energy Materials and Solar Cells* **2013**, *113*, 26–30.

(37) Xiao, D.; Li, X.; Wang, D.; Li, Q.; Shen, K.; Wang, D. CdTe thin film solar cell with NiO as a back contact buffer layer. *Solar Energy Materials and Solar Cells* **2017**, *169*, 61–67.

(38) Ghosh, B.; Purakayastha, S.; Datta, P.; Miles, R.; Carter, M.; Hill, R. Formation of a stable ohmic contact to CdTe thin films through the diffusion of P from Ni-P. *Semiconductor science and technology* **1995**, *10*, 71–76.

(39) Metzger, W.; Grover, S.; Lu, D.; Colegrove, E.; Moseley, J.; Perkins, C.; Li, X.; Mallick, R.; Zhang, W.; Malik, R.; Kephart, J.; Jian, C.; Kuciauskas, D.; Albin, D.; Al-Jassim, M.; Xiong, G.; Gloeckler, M. Exceeding 20% efficiency with in situ group V doping in polycrystalline CdTe solar cells. *Nature Energy* **2019**, *4*, 837–845.

(40) Diamond, A. M.; Corbellini, L.; Balasubramaniam, K.; Chen, S.; Wang, S.; Matthews, T. S.; Wang, L.-W.; Ramesh, R.; Ager, J. W. Copper-alloyed ZnS as a p-type transparent conducting material. *physica status solidi (a)* **2012**, *209*, 2101–2107.

(41) Xu, X.; Bullock, J.; Schelhas, L. T.; Stutz, E. Z.; Fonseca, J. J.; Hettick, M.; Pool, V. L.; Tai, K. F.; Toney, M. F.; Fang, X.; Ager, J. Chemical bath deposition of p-type transparent, highly conducting $(CuS)_x$:$(ZnS)_{1-x}$ nanocomposite thin films and fabrication of Si heterojunction solar cells. *Nano letters* **2016**, *16*, 1925–1932.

(42) Woods-Robinson, R.; Cooper, J. K.; Xu, X.; Schelhas, L. T.; Pool, V. L.; Faghaninia, A.; Lo, C. S.; Toney, M. F.; Sharp, I. D.; Ager, J. W. P-Type Transparent Cu-Alloyed ZnS Deposited at Room Temperature. *Advanced Electronic Materials* **2016**, *2*, 1500396.

(43) Woods-Robinson, R.; Han, Y.; Mangum, J. S.; Melamed, C. L.; Gorman, B. P.; Mehta, A.; Persson, K. A.; Zakutayev, A. Combinatorial Tuning of Structural and Optoelectronic Properties in $Cu_xZn_{1-x}S$. *Matter* **2019**, *1*, 862–880.

(44) Subedi, K. K.; Bastola, E.; Subedi, I.; Song, Z.; Bhandari, K. P.; Phillips, A. B.; Podraza, N. J.; Heben, M. J.; Ellingson, R. J. Nanocomposite $(CuS)_x(ZnS)_{1-x}$ thin film back contact for CdTe solar cells: Toward a bifacial device. *Solar Energy Materials and Solar Cells* **2018**, *186*, 227–235.

(45) Becker, J.; Xu, X.; Woods-Robinson, R.; Campbell, C.; Lassise, M.; Ager, J.; Zhang, Y.-H. CuZnS hole contacts on monocrystalline CdTe solar cells. *Photovoltaic Specialist Conference (PVSC), 2017 IEEE 44th* **2017**, 1–3.

(46) Meysing, D. M.; Reese, M. O.; Warren, C. W.; Abbas, A.; Burst, J. M.; Mahabaduge, H. P.; Metzger, W. K.; Walls, J. M.; Lonergan, M. C.; Barnes, T. M.; Wolden, C. A. Evolution of oxygenated cadmium sulfide (CdS: O) during high-temperature CdTe solar cell fabrication. *Solar Energy Materials and Solar Cells* **2016**, *157*, 276–285.

(47) Richards, W. D.; Miara, L. J.; Wang, Y.; Kim, J. C.; Ceder, G. Interface stability in solid-state batteries. *Chemistry of Materials* **2015**, *28*, 266–273.

(48) Jain, A.; Ong, S. P.; Hautier, G.; Chen, W.; Richards, W. D.; Dacek, S.; Cholia, S.; Gunter, D.; Skinner, D.; Ceder, G.; Persson, K. A. Commentary: The Materials Project: A materials genome approach to accelerating materials innovation. *Apl Materials* **2013**, *1*, 011002.

(49) Blöchl, P. E. Projector augmented-wave method. *Phys. Rev. B* **1994**, *50*, 17953.

(50) Kresse, G.; Joubert, D. From ultrasoft pseudopotentials to the projector augmented-wave method. *Phys. Rev. B* **1999**, *59*, 1758–1775.

(51) Kresse, G.; Hafner, J. Ab initio molecular dynamics for liquid metals. *Phys. Rev. B* **1993**, *47*, 558–561.

(52) Kresse, G.; Furthmüller, J. Efficient iterative schemes for ab initio total-energy calculations using a plane-wave basis set. *Phys. Rev. B* **1996**, *54*, 11169.

(53) Perdew, J. P.; Burke, K.; Ernzerhof, M. Generalized gradient approximation made simple. *Phys. Rev. Letters* **1996**, *77*, 3865.

(54) Ong, S. P.; Richards, W. D.; Jain, A.; Hautier, G.; Kocher, M.; Cholia, S.; Gunter, D.; Chevrier, V. L.; Persson, K. A.; Ceder, G. Python Materials Genomics (pymatgen): A robust, open-source python library for materials analysis. *Comput. Mater. Sci.* **2013**, *68*, 314–319.

(55) Gutowski, J.; Sebald, K.; Voss, T. In *New Data and Updates for III-V, II-VI and I-VII Compounds*; Rössler, U., Ed.; Springer Berlin Heidelberg: Berlin, Heidelberg, 2010; pp 479–480.

(56) Liu, G.; Schulmeyer, T.; Brötz, J.; Klein, A.; Jaegermann, W. Interface properties and band alignment of Cu_2S/CdS thin film solar cells. *Thin Solid Films* **2003**, *431*, 477–482.

(57) Fritsche, J.; Schulmeyer, T.; Kraft, D.; Thißen, A.; Klein, A.; Jaegermann, W. Utilization of sputter depth profiling for the determination of band alignment at polycrystalline CdTe/CdS heterointerfaces. *Applied physics letters* **2002**, *81*, 2297–2299.

(58) Zhao, Y.; Boccard, M.; Liu, S.; Becker, J.; Zhao, X.-H.; Campbell, C. M.; Suarez, E.; Lassise, M. B.; Holman, Z.; Zhang, Y.-H. Monocrystalline CdTe solar cells with open-circuit voltage over 1 V and efficiency of 17%. *Nature Energy* **2016**, *1*, 16067.

(59) Nazem, H.; Dizaj, H. P.; Gorji, N. E. Modeling of Jsc and Voc versus the grain size in CdTe, CZTS and Perovskite thin film solar cells. *Superlattices and Microstructures* **2019**, *128*, 421–427.

(60) Iida, H.; Shiba, N.; Mishuku, T.; Karasawa, H.; Ito, A.; Yamanaka, M.; Hayashi, Y. Efficiency of the a-Si: H solar cell and grain size of SnO 2 transparent conductive film. *IEEE Electron Device Letters* **1983**, *4*, 157–159.

(61) Dobson, K. D.; Visoly-Fisher, I.; Hodes, G.; Cahen, D. Stability of CdTe/CdS thin-film solar cells. *Solar Energy Materials and Solar Cells* **2000**, *62*, 295–325.

(62) First Solar Series 6^{TM}: next generation thin film solar technology. First Solar, 2020.

(63) Koishiyev, G. T.; Sites, J. R.; Kulkarni, S. S.; Dhere, N. G. Determination of back contact barrier height in Cu(In,Ga)(Se,S)$_2$ and CdTe solar cells. *2008 33rd IEEE Photovoltaic Specialists Conference* **2008**, 1–3.

(64) Duenow, J. N.; Dhere, R. G.; Li, J. V.; Young, M. R.; Gessert, T. A. Effects of back-contacting method and temperature on CdTe/CdS solar cells. *2010 35th IEEE Photovoltaic Specialists Conference* **2010**, 001001–001005.

(65) Sze, S. M.; Ng, K. K. *Physics of semiconductor devices*; John Wiley & Sons, 2006.

(66) Gessert, T.; Metzger, W.; Dippo, P.; Asher, S.; Dhere, R.; Young, M. Dependence of carrier lifetime on Cu-contacting temperature and ZnTe: Cu thickness in CdS/CdTe thin film solar cells. *Thin Solid Films* **2009**, *517*, 2370–2373.

(67) Demtsu, S.; Albin, D.; Sites, J.; Metzger, W.; Duda, A. Cu-related recombination in CdS/CdTe solar cells. *Thin Solid Films* **2008**, *516*, 2251–2254.

(68) Reidy, C. F. Heterojunction Assisted Impact Ionization at the ZnS/Si Interface and $Cu_{10}Te_4S_{13}$ Photodiodes. Ph.D. thesis, Oregon State University, 2018.

(69) Chu, T.; Chu, S. S.; Britt, J.; Ferekides, C.; Wu, C. Cadmium zinc sulfide films and heterojunctions. *Journal of Applied Physics* **1991**, *70*, 2688–2693.

(70) Sato, H.; Hirai, T.; Komasawa, I. Mechanism of formation of composite CdS-ZnS ultrafine particles in reverse micelles. *Industrial & engineering chemistry research* **1995**, *34*, 2493–2498.

(71) Wolden, C. A.; Abbas, A.; Li, J.; Diercks, D. R.; Meysing, D. M.; Ohno, T. R.; Beach, J. D.; Barnes, T. M.; Walls, J. M. The roles of ZnTe buffer layers on CdTe solar cell performance. *Solar Energy Materials and Solar Cells* **2016**, *147*, 203–210.

(72) Du, S.; Zhu, L.; Li, W.; Zhang, J.; Wu, L.; Wang, W. Bilayered ZnTe/$Cu_{1.4}Te$ alloy thin films as a back contact for CdTe solar cells. *Solar Energy* **2019**, *185*, 262–269.

(73) Kitabayashi, S.; Shiina, Y.; Murata, A.; Okamoto, T.; Wada, T. Fabrication of p-type SrCuSeF/n-type In_2O_3: Sn bilayer ohmic tunnel junction and its application to the back contact of CdS/CdTe solar cells. *Japanese Journal of Applied Physics* **2017**, *56*, 08MC18.

(74) Bhushan, B.; Luo, D.; Schricker, S. R.; Sigmund, W.; Zauscher, S. *Handbook of nanomaterials properties*; Springer Science & Business Media, 2014.

(75) De Wolf, S.; Descoeudres, A.; Holman, Z. C.; Ballif, C. High-efficiency silicon heterojunction solar cells: A review. *green* **2012**, *2*, 7–24.

(76) Bullock, J.; Hettick, M.; Geissbühler, J.; Ong, A. J.; Allen, T.; Sutter-Fella, C. M.; Chen, T.; Ota, H.; Schaler, E. W.; De Wolf, S.; Ballif, C. Efficient silicon solar cells with dopant-free asymmetric heterocontacts. *Nature Energy* **2016**, *1*, 15031.

(77) Sacchetto, D.; Jeangros, Q.; Christmann, G.; Barraud, L.; Descoeudres, A.; Geissbühler, J.; Despeisse, M.; Hessler-Wyser, A.; Nicolay, S.; Ballif, C. ITO/MoO_x/a-Si: H (i) hole-selective contacts for silicon heterojunction solar cells: degradation mechanisms and cell integration. *IEEE Journal of Photovoltaics* **2017**, *7*, 1584–1590.

(78) Siol, S.; Dhakal, T. P.; Gudavalli, G. S.; Rajbhandari, P. P.; DeHart, C.; Baranowski, L. L.; Zakutayev, A. Combinatorial reactive sputtering of In_2S_3 as an alternative contact layer for thin film solar cells. *ACS applied materials & interfaces* **2016**, *8*, 14004–14011.